Bioinspiration & Biomimetics

PAPER

Fish-like aquatic propulsion studied using a pneumatically-actuated soft-robotic model

Z Wolf[1,4], A Jusufi[2], D M Vogt[3] and G V Lauder[1]

[1] Department of Organismic and Evolutionary Biology, Harvard University, 26 Oxford Street, Cambridge, MA 02138, United States of America
[2] Max Planck Institute for Intelligent Systems, Heisenbergstraße 3, Stuttgart 70769, Germany
[3] Wyss Institute, Harvard University, 60 Oxford Street, Cambridge, MA 02138, United States of America
[4] Author to whom any correspondence should be addressed.

E-mail: rzwolf@g.harvard.edu

RECEIVED
13 February 2020

REVISED
16 April 2020

ACCEPTED FOR PUBLICATION
24 April 2020

PUBLISHED
4 June 2020

Keywords: soft robotics, fish locomotion, model, active swimming

Supplementary material for this article is available online

Abstract

Fish locomotion is characterized by waves of muscle electrical activity that proceed from head to tail, and result in an undulatory pattern of body bending that generates thrust during locomotion. Isolating the effects of parameters like body stiffness, co-activation between the right and left sides of the body, and frequency on thrust generation has proven to be difficult in live fishes. We use a pneumatically-actuated fish-like model to investigate how these parameters affect locomotor force generation. We measure thrust as well as side forces and torques generated during propulsion. Using a statistical linear model we examine the effects of input parameter combinations on thrust generation. We show that both stiffness and frequency substantially affect swimming kinematics, and that there are complex interactive effects of these two parameters on thrust. The stiffer the backbone the more impact that increasing frequency has on thrust production. For stiffer models, increasing frequency resulted in higher values for both thrust and lateral forces. Large side forces reduce swimming efficiency but this effect could be mitigated by decreasing undulatory wavelength and allowing appropriate phasing of left and right body movements to reduce amplitudes of side force.

1. Introduction

Robotics are becoming increasingly integrated into biological studies. Robotic models can be used either to replicate behaviors or properties observed in the biological system or to gain new insights into the biological system itself (Gravish and Lauder 2018), and the complexity of these bio-inspired robotic models can vary from simple models useful for analyzing individual features of organisms, to complex autonomous models that learn to operate themselves (Shelton *et al* 2014, Coral *et al* 2018, Long 2012). Both simple and complex models have been used to study fish locomotion, as it is difficult to isolate or modify the features of living fishes.

One specific area of ongoing research in fish locomotion is the study of passive and active swimming systems. Passive propulsion occurs when morphological features of a fish interact with the surrounding flow to generate motion, in the absence of muscle activation. This phenomenon can be observed in dead fish. When positioned behind cylinders in flow, which generate a Karman vortex wake, fish bodies are undulated due to fluid interacting with the body form, rather than through muscle activation (Liao 2004). This can be simulated in a model by activating the leading edge of a foil shim with an external motor—the length of the foil will exhibit undulatory motion due to the water interacting on the foil (Fish and Lauder 2006, Lauder *et al* 2012, Lauder *et al* 2011). In contrast, active swimming is the result of the fish imparting momentum to surrounding flow through muscular activation of the fins or body (Fish and Lauder 2006, Lauder 2015, Shadwick and Gemballa 2006). While it is understood that aquatic organisms use both passive and active mechanisms while swimming, especially at lower speeds, previous studies have largely focused on either the passive or the active swimming and the associated components.

Body stiffness is an important component of both active and passive aspects of swimming (McHenry *et al* 1995, Long *et al* 1994, Long 1998). Passive stiffness is imparted through the integument, soft tissue such as tendons, ligaments, and muscle, as well as hard structures such as the vertebral column and fin rays. Active stiffness is generated and modified mostly through muscle activation, can be altered quickly during swimming, and is often accompanied by a change in swimming speed (Long *et al* 1996, Lauder 2011, Colgate and Lynch 2004). Previous studies using electrically-stimulated dead fish suggest that fish need to increase their flexural stiffness, via muscle activation, in order to swim at higher frequencies effectively (McHenry *et al* 1995, Long *et al* 1996, MacIver *et al* 2004). The increased work involved in muscular stiffening of the body may be mitigated by a reduction in drag while swimming, an increase in thrust, or both (Barrett *et al* 1999, Mcletchie 2003), although the energetic consequences of changing body stiffness are still not well understood.

Flexible foil models have been useful for reducing the complexity of the fish body to a passive plastic sheet of given flexural stiffness and shape, thus allowing controlled experiments that vary specific features of a swimming body (McHenry *et al* 1995, Feilich and Lauder 2015, Lucas *et al* 2015, Lauder 2011, Shelton *et al* 2014, Wen and Lauder 2013). These tractable models allow for precise control of heave, pitch, and frequency at the leading foil edge, and the foils are easily cut from flexible plastic material. However, this foil propulsive system is activated using an external motor, and most resultant undulation of the foil is due to the effect of water pushing on the foil as the leading edge moves through the fluid. In contrast, hard robotic fish models actively swim and have begun to incorporate active stiffness control (Ziegler *et al* 2011, Li *et al* 2018). Ultimately, however, these models are often accompanied by long manufacturing times and complicated control systems, and are challenging to alter to examine the effects of different body features, and few have controlled the stiffness pneumatically (Katzschmann *et al* 2018).

Soft robotic systems offer an opportunity to construct a model locomotor system that is both actively swimming and also readily controlled and manufactured. Jusufi *et al* (2017) designed a soft-robotic fish-like model to investigate mechanisms for body stiffness control and the effect on undulatory locomotion at different flow speeds. Soft fluidic actuators, or pneunets (Mosadegh *et al* 2014, Zhou and Li 2019), were attached bilaterally to a flexible backbone foil, and activated using compressed air (Jusufi *et al* 2017). Based on measurement of robot swimming performance in a recirculating flow tank, they found a non-linear relationship between forward net thrust and amplitude of excursion with activation frequency. Additionally, Jusufi *et al* (2017) investigated the effect of bilateral co-contraction between the pneunets and found that an antagonistic overlap of roughly 3% yielded a higher net thrust than no or more overlap. This study established this soft robotic system as a plausible model for studying fish locomotion. Moreover, hyperelastic soft sensors containing liquid metal gallium indium within microchannels were tested on two locations along the body of a soft robotic fish, finding that sensor readings captured the undulation kinematics. Such input can be used for sensory feedback during swimming and closed loop control (Wright *et al* 2019, Souri *et al* 2020). The model also represents a tractable platform for investigating the effects of not only passive flexural stiffness, imparted by the flexible foil backbone, but also variable active stiffness, modulated using pneumatic air pressure in the pneunets. The ability to vary active stiffness in any capacity in a swimming robotic platform is a particularly useful attribute of this experimental platform.

The goals of this study are to build upon the approach of Jusufi *et al* (2017) by creating three separate model 'pneufish' each with a different stiffness of central backbone and quantitatively investigating the interaction effects among activation frequency, passive flexural stiffness, and active stiffness modulation through maximum and minimum pressure. In addition, we introduce use of a statistical linear model to explore the interactions between stiffness and frequency and improve our understanding of the control system and pneufish swimming performance. By measuring side forces and torques generated by locomotion we are able to address the hypothesis that increasing body stiffness results in increased side forces which may limit propulsive performance at high frequencies.

2. Materials and methods

2.1. Design and fabrication of the pneufish

The soft fluidic actuators, or pneunets, were manufactured using the methodology as described in Mosadegh *et al* (2014) and Jusufi *et al* (2017) (figures 1(A) and (B)). Uncured silicone (Dragon-Skin 20; Smooth-On, Inc., Easton, PA) was poured into two molds 3D-printed with a polyjet printer (Objet Geometries, Stratasys, MN): a dorsal section with chambers, and a ventral plate mold. The elastomer was cured at 60°C for 25 min. After a cooling period, the two halves of the pneunet design were combined using a thin layer of Dragon-Skin, and allowed to cure at room temperature for a minimum of 4 h. Pneunet functionality (complete inflation of every chamber; no leaks) was confirmed by inserting a 26G$\times$ $\frac{5}{8}''$ needle into a terminal chamber and inflating with a syringe. Once tested, a luer-to-tubing polypropylene input valve (World Precision Instruments, Sarasota, FL)) was permanently attached to

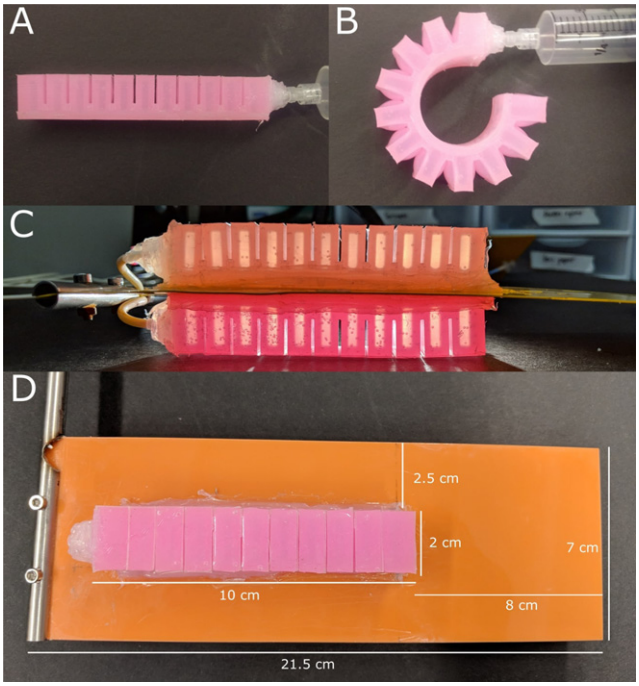

Figure 1. Pneufish assembly. (A) and (B) show an un-inflated and inflated pneunet, respectively. Each pneunet, when inflated, produces a net curvature toward the inner surface. (C) shows an assembled pneufish viewed from below and illuminated from behind to reveal the individual chambers within each pneunet. Each pneunet has 11 chambers. (D) shows a lateral (side) view of the assembled pneufish model, with the pneunet located on the flexible backbone foil, toward the housing rod, to produce a posterior 'tail.' Measurements for symmetric pneufish assembly are shown in white.

one end of each pneunet using silicone epoxy (Sil-Poxy™; Smooth-On, Inc., Easton, PA) (figures 1(A) and (B)).

The pneufish was assembled by attaching two pneunets bilaterally to a flexible thick shim stock (Artus, Inc.). The pneunets were glued in place using silicone epoxy. Pneufish of varying passive stiffnesses were created by using plastic sheets cut from shim stock of varying flexural stiffness values. Pneunets were oriented with the input valves located anteriorly. Static-dissipative polyurethane tubing (1/16″ ID, 1/8″ OD; McMaster-Carr, Robbinsville, NJ) was attached to the input valves. The plastic backbone and tubing were mounted on a metal housing rod that inserted into a Nano 17 six-axis force/torque transducer (ATI Industrial Automation, Apex, NC). The housing rod was secured to an aluminum crossbeam above the flow tank to hold the entire apparatus in place (figures 1(C) and (D)). The head of the pneufish model was held stationary in the tank, while the body of the pneufish generated its own undulatory motion as a result of alternating pressure changes introduced by digital pneumatic controllers. In order to simplify the design and facilitate the changing of backbone material, which was necessary for testing models of different stiffnesses, we removed the 3D-printed anterior cuff present on the previous version of this model developed by Jusufi *et al* (2017).

Pneunets were activated individually using compressed air ranging between 0.5 kPa and 1.00 kPa. Air pressure was controlled using digital pressure regulators (Model ITV00050-2U(B)L, SMC Pneumatics, Yorba Linda, CA), which were operated by a microcontroller circuit board (Arduino, Uno, SmartProjects, Italy). Pulse-width modulation and a low-pass RC filter (100 nF capacitor and 16.1 kΩ resistor, resulting in a cut-off frequency of 98.8 Hz) were used to convert the Arduino's output signal to a value between 0–5 V, the input signal range of the digital pressure regulators. Due to manufacturing differences in both the pneunets and regulators, there were small discrepancies between the desired pressure value set using the Arduino code and the pressured outputted by the individual pressure regulators and ultimately the resultant curvature of the pneunets. We measured the pressure outputs for each regulator for many given input values with a pressure sensor (BSPB010-EV002-A00A0B-S4; Balluff, Inc., Florence, KY) and selected two regulators with similar input–output variations to control the separate pneunets on each side of the pneufish.

The Arduino code contains a variable that controls the step size and frequency of air inflation. For example, at 0.25 Hz, pneunets could be inflated with smaller bursts of air every 800 ms, or in two larger bursts of air every 2 s. To test the effect of this inflation rate, or 'Step Time' parameter, we compared 250 ms intervals (less air more frequently) with 500 ms (more air less frequently) intervals, and the results are shown in figure 2. The 500 ms value consistently produced higher thrust values when

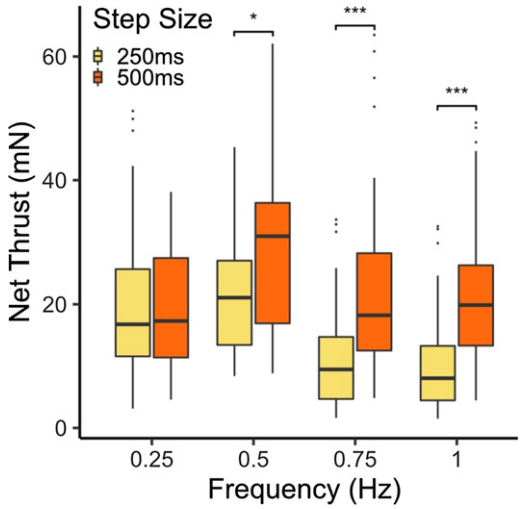

Figure 2. The effect of inflation rates on thrust production. Two 'step time' inputs were compared at all frequencies, and binned for all foil stiffnesses, maximum and minimum pressures, and zero flow speed. Step time becomes increasingly important as frequency increases, and as the total time the pneunet has to inflate and the pneufish has to oscillate, decreases. In this figure and any subsequent boxplot figures, the bottom and top of the box represent the 25th and 75th percentile of the data and the whisker lengths are the default setting of 1.5 × IQR. $^{*}P < 0.05$, $^{***}P < 0.001$.

Table 1. Parameter space table. The three flexural stiffness values will be referred to as the flexible, medium, and stiff foil backbones, respectively. Step time and pneunet orientation parameters are not shown, because they were tested within a subset of this larger parameter space.

Parameter	Values
Frequency (Hz)	0.25 0.5 0.75 1.0
Maximum pressure (kPa)	0.5 0.75 1.0
Minimum pressure (%)	0 5 10 25
Foil stiffness	1.02×10^{-3} N m^2 (flexible) 3.12×10^{-3} N m^2 (medium) 1.55×10^{-2} N m^2 (stiff)
Flow speed (cm s^{-1})	0 5.3

examined across the parameter space at 0 cm s^{-1} flow speed. Therefore, we chose to conduct the rest of the parameter space exploration using 500 ms step intervals only.

2.2. Parameter space

Pneufish swimming performance was evaluated across a large parameter space (table 1), designed with both biologically-relevant values and mechanical limitations of the digital pressure regulators in mind.

Studies were conducted in a flow tank with working dimensions 26 cm by 26 cm by 80 cm. Jusufi *et al* (2017) definitively showed a linear, negative relationship between increasing flow speed (from 0 cm s^{-1} to 20 cm s^{-1}) and thrust production. While the effect on thrust and the interaction with other parameters may be large, it could be safely assumed that the nature of the relationship with regards to thrust and increasing flow speed would not change. Therefore, we chose to include only two flow speeds in our parameter space: 0 cm s^{-1} (no flow), and 5.3 cm s^{-1}, which was high enough that drag was larger than the pneufishes thrust production at certain parameter combinations. In order to maintain the parameter space at a manageable size, other flow speeds were not investigated.

The pneufish swam at four frequencies: 0.25 Hz, 0.5 Hz, 0.75 Hz and 1.0 Hz. These are realistic steady swimming frequencies for fish moving at slow to slow/moderate speeds (Bainbridge 1958, Tytell and Lauder 2004, Tytell 2006, Drucker 1996). The digital pressure regulators were incapable of effectively modulating air pressure at higher frequencies, and their performance limited this parameter range.

Passive stiffness of the pneufish was modified by using shim stock of varying flexural stiffness: 1.02×10^{-3} Nm^2 ('flexible'), 3.12×10^{-3} Nm^2 ('medium'), and 1.55×10^{-2} Nm^2 ('stiff'). These flexural stiffness values are similar to that of real fish estimated during slow speed locomotion as discussed by Shelton *et al* (2014).

The digital pressure regulators allow for the control of not just the air pressure during pneunet activation ('maximum pressure (kPa)'), but also the amount of air remaining in the pneunet while 'inactive' (i.e., when the pneunet on the other side of the plastic backbone is actively inflating). The amount of remaining air is called the 'minimum pressure' parameter and is a percentage of whatever the maximum pressure value is at that parameter combination. By modulating the minimum amount of air left in the pneunets, we can effectively modulate the overall stiffness of the pneufish both post-manufacture and during swimming. This principle has been demonstrated by Jusufi *et al* (2017), whereby increasing bilateral pressure increased the stiffness of the overall apparatus. Because the minimum pressure is actively opposing the maximum pressure on the opposite side of the pneufish, it was desirable to keep the ratio of opposition the same (e.g. 5%, 10%) rather than use consistent values for minimum pressure (e.g. 0.015 kPa, 0.2 kPa).

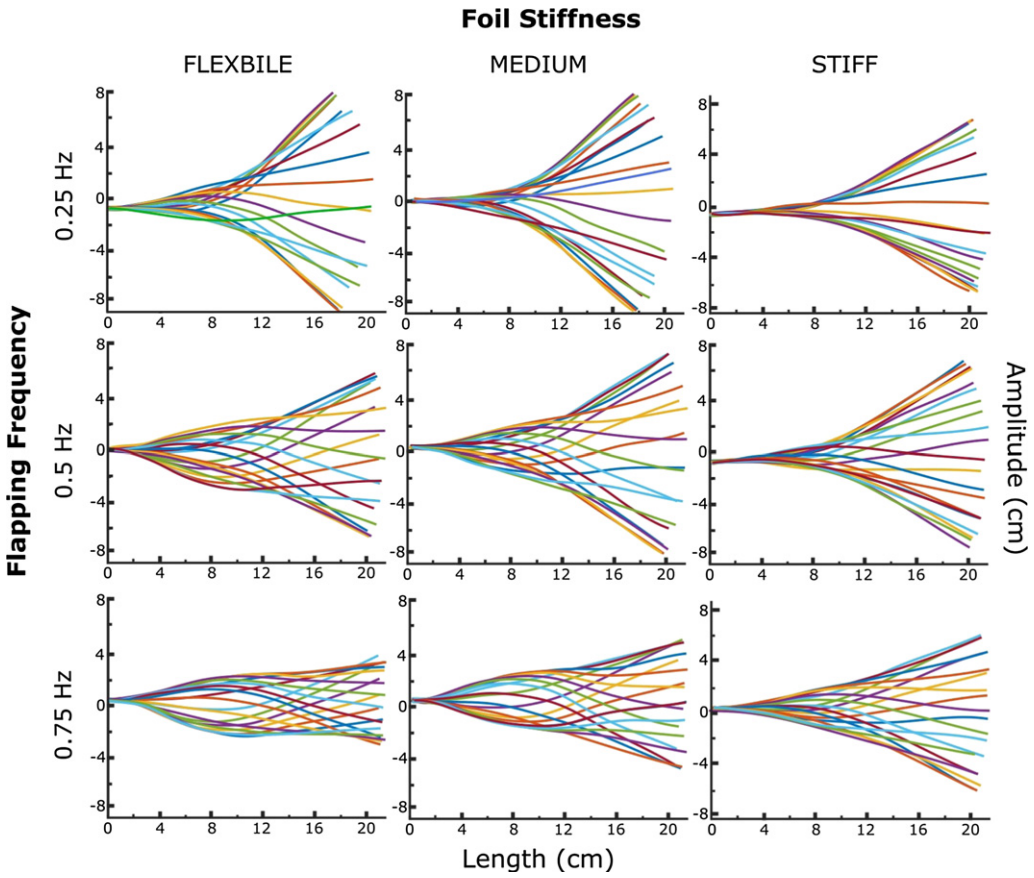

Figure 3. Kinematics of swimming pneufish over a single motion cycle. Leading edge is on the left. For each sample, the maximum pressure was 0.75 kPa, minimum pressure was 0%, flow speed was 5.3 cm s^{-1}.

2.3. Data acquisition and analysis

Swimming kinematics were collected through ventral high-speed videography, with a Photron PCI-1024 high-speed video camera (one megapixel resolution, 500 frames per second). Swimming midlines were generated using a proprietary script in Matlab R2016b (The Mathworks, Natick, Mass. USA), and the oscillation tail-tip amplitudes were measured using ImageJ (Schneider *et al* 2012). Midline motions are a useful diagnostic tool in experiments on the swimming of fish and fish-like models because they allow us to visualize the undulatory motion of the machine/animal in question and compare the effect of altering control parameters.

Concurrently with videography data, the six-axis force/torque transducer located on the metal housing rod recorded thrust and torque produced by the swimming pneufish and the surrounding flow. The *x*-axis is oriented parallel to flow (positive axis points forward in the flow tank, negative points backwards), the *y*-axis is perpendicular to flow (or 'laterally'), and the *z*-axis is oriented along the housing rod (positive values pointing upwards). Force/torque measurements were taken at 1000 Hz for 10 s per single data sequence collection, and each parameter combination shown in table 1 was measured in quadruplicate. Positive net thrust value (averaged over the 10 s collection period) indicates the pneufish would be accelerating forward through the water column if untethered. If negative, drag would be overpowering the pneufish, accelerating it backwards in the water column. By definition, net *x*-force values are zero at self-propelled speed (Lauder *et al* 2011).

Mathematica (Wolfram Research Inc. 2019) was used to process the raw force/torque data using a low-pass filter (the function lowpass filter, $\omega_c = 0.003$), which allowed us to find peak-to-peak oscillation amplitudes for $F_{\hat{x}}$, $F_{\hat{y}}$, and $T_{\hat{z}}$. $F_{\hat{x}}$ is the net thrust, as described above, $F_{\hat{y}}$ is the lateral force generated during swimming, and $T_{\hat{z}}$ is the torque produced on the housing rod or 'head' of the (pneu)fish. Measurements of the peak-to-peak force oscillations provide an indication of how unsteady force generation is for any one parameter combination, and indicate the extent to which the pneufish center of mass would oscillate if the pneufish were free-swimming (Wen and Lauder 2013). Both the raw and processed data were then analyzed with R (R Core Team 2013).

We made a generalized linear model (glm, baseR) of the thrust data, with the following input parameters: frequency, maximum activation pressure, minimum activation pressure, flow speed, backbone foil stiffness, and select interactions. We used a linear model to understand the relative importance

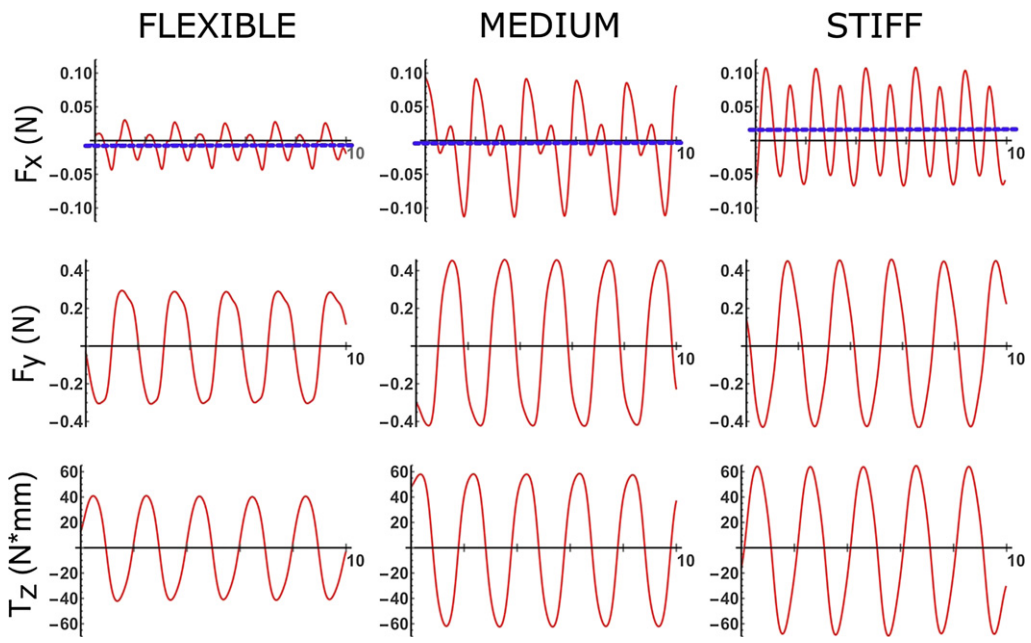

Figure 4. Representative thrust, lateral force, and torque through time (in seconds) for three foil stiffnesses. Blue-dotted lines represent mean thrust values for the cycle. These data are from the following parameter combination: flow speed: 5. 3cm s^{-1}; maximum pressure: 0.75 kPa; minimum pressure: 0%, and frequency: 0.75 Hz.

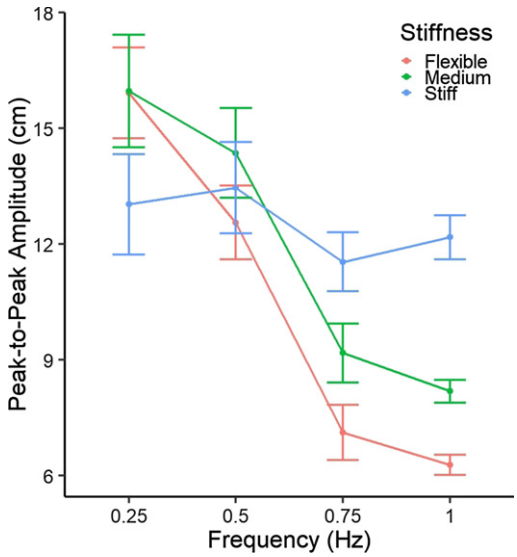

Figure 5. Tail tip amplitude of the pneufish swimming at 5.3 cm s^{-1} flow speed. Error bars represent standard error across all maximum and minimum pressure values. As frequency increases, the stiff foil shows minimal variation in oscillation amplitude, while both the flexible and medium foil stiffnesses decrease in oscillation amplitude.

of each variable in determining thrust production (Gelman and Hill 2007). Input parameters were transformed into factors and not treated continuously, thus allowing for any non-linear effects to become apparent without fitting a non-linear model. To compare the relative fits of various models, we performed an Akaike Information Criteria (AIC) analysis, using the stepAIC function, adjusting the model as necessary (Venables and Ripley 2002). An AIC analysis compares the quality of several models to each other by, in this case, subtracting parameter inputs to reduce the complexity (Venables and Ripley 2002).

3. Results

3.1. Swimming kinematics

The swimming performance of the pneufish model was characterized across a parameter space of 288 parameter combinations. For the flexible and medium backbone foils, increasing the activation frequency decreased the amplitude and streamlined the motion producing a smaller frontal area (figure 3). However, for the stiffest backbone foil, increasing the amplitude had little apparent change on the midline kinematics of the pneufish. No parameter combination resulted in midlines that demonstrated 'true undulatory motion'; i.e., the oscillation wavelength of the foil never exceeded the length of the pneufish foil ($\lambda \leqslant L$).

In figure 4, we show example collected data for $F_{\hat{x}}$, $F_{\hat{y}}$, and $T_{\hat{z}}$ across three backbone foil stiffnesses. Thrust for pneufish with medium and stiff backbones increases compared to the flexible backbone, as do side forces and z-torque. The pneufish with the intermediate backbone stiffness self-propels at the imposed flow speed of 5.3 cm s^{-1}, while the flexible and stiff backbones result in thrust, respectively, less than and greater than self-propulsion.

Tail-tip amplitude of the flexible and medium stiffness pneufish models decreased with increasing activation frequency (figure 5). However, the stiff pneufish did not experience this negative linear relationship with frequency.

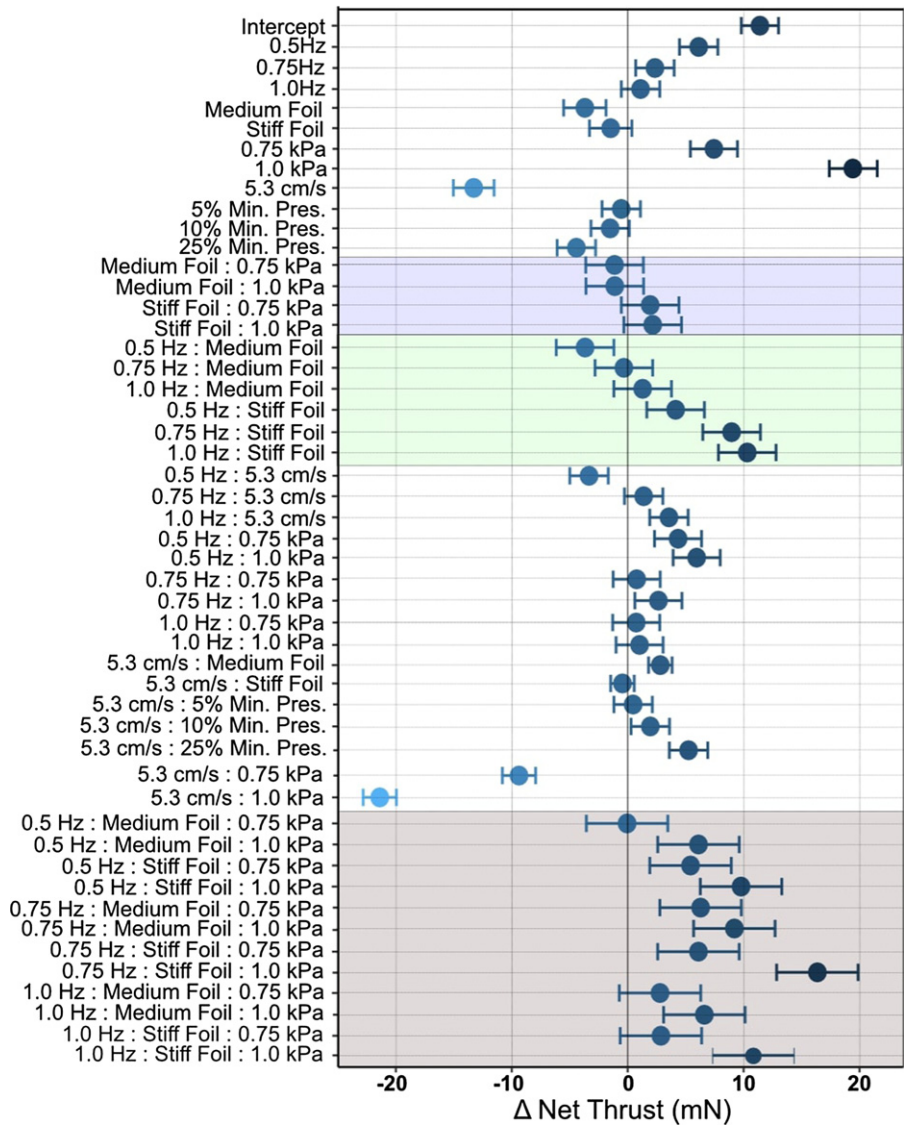

Figure 6. Regression coefficients graph shows the effect of each parameter and parameter interaction on thrust production. The *x*-axis represents change (in mN) from the baseline parameter combination: 0.25 Hz, flexible backbone foil, 0.5 kPa maximum pressure, 0 cm s^{-1} flow speed, and 0% minimum pressure. All parameter combinations that do not have 'medium' or 'stiff' listed are for the flexible case. The *y*-axis consists of each parameter and parameter interaction combination included in the linear model (see text for further discussion). Whiskers represent the 95% confidence interval; variables with confidence intervals intercepting the reference line at 0 mN are unlikely to substantially influence thrust production. Highlighted regions show interactions between stiffness and max pressure (blue box), stiffness and frequency (green box), and stiffness, frequency, and maximum air pressure (gray box).

3.2. Parameter space analysis

A priori we intuited that amplitude, while not an input, would serve as a good predictor of thrust. Videos, and therefore amplitude data, were collected for one replicate of the four total replicates for each parameter combination. We performed a linear regression to predict net thrust based solely on amplitude, $F_{\hat{x}} \sim$ amplitude. A significant model was found: predicted net thrust was equal to $-2.71 + 1.21$(amplitude) mN, where amplitude is measured in centimeters. The amplitude coefficient has a p-value of 1.1×10^{-13} (where $p < 0.01$ is significant). However, this model had an adjusted R^2 value of 0.17. We then expanded this model to include flow speed and the interaction effect: $7.09 + 1.13$(amplitude) $- 8.38$(flowspeed) $-$ 0.79(amplitude : flowspeed), where amplitude was measured in centimeters and flow speed was binary, representing the two tested flow speeds. The *p*-values of both amplitude, flow speed, and the interaction effect were highly significant: 7.15×10^{-13}, 0.0099, and 0.0011, respectively. The adjusted R^2 value for this second model was 0.55. We then attempted to find a model that explained as much variance as possible.

The best-fit model, as indicated by AIC (supplementary tables 1 and 2) (https://stacks.iop.org/BB/15/046008/mmedia), is as follows, (Gelman and Hill 2007, Venables and Ripley 2002):

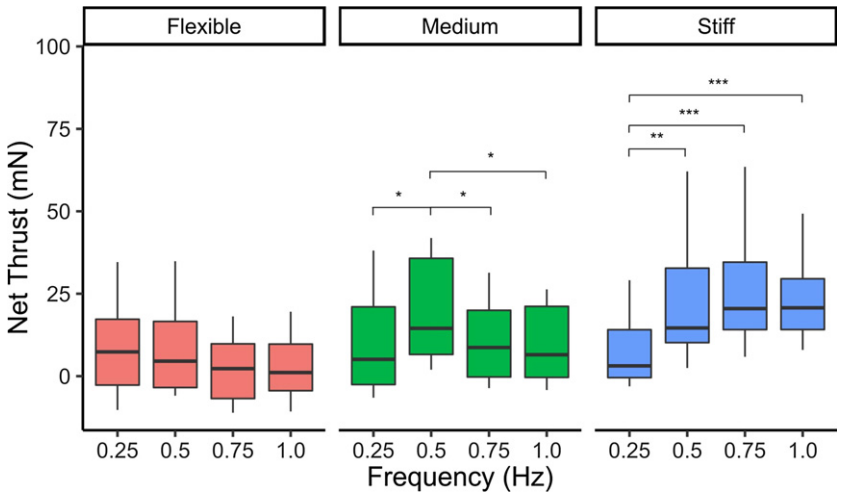

Figure 7. The stiffer the foil, the more impact increasing frequency has on thrust production. For the flexible foil, increasing the frequency alone produces no significant difference in thrust production. For the medium and stiff foils, increasing the frequency yields significant increases in thrust production, except for the increase between 0.75 Hz and 1.0 Hz. $^{*}P < 0.05$, $^{**}P < 0.01$, $^{***}P < 0.001$.

$$\begin{aligned} F_{\hat{x}} \sim\ & \text{frequency} + \text{flowspeed} + \text{foilstiffness} + \text{maximumpressure} + \text{minimumpressure} \\ & + \text{frequency} * \text{flowspeed} + \text{frequency} * \text{foilstiffness} + \text{frequency} * \text{maximumpressure} \\ & + \text{flowspeed} * \text{foilstiffness} + \text{flowspeed} * \text{minimumpressure} \\ & + \text{foilstiffness} * \text{maximumpressure} \\ & + \text{foilstiffness} * \text{maximumpressure} * \text{frequency} \end{aligned} \tag{1}$$

AIC removed amplitude as a predictor (supp. table 1). This best-fit model, when applied to both the full data set and the subset for which amplitude was collected, had an adjusted R^2 value of 0.97 and 0.96, respectively. The coefficients for each predictor in the model indicate the size of the effect of each parameter and parameter interactions on thrust production (figure 6; *p*-values for each coefficient are shown in supp. table 3). The intercept parameter combination for this graph is: 0.25 Hz, flexible, 0.5 kPa maximum pressure, 0 cm s^{-1} flow speed, 30% activation overlap and 0% minimum pressure. The value of the coefficient (its position on the *x*-axis) represents the average increase or decrease of net thrust conferred by changing from the intercept parameter value to the new value. For example, increasing the frequency from 0.25 Hz to 0.5 Hz slightly decreases net thrust, but the 95% confidence interval intercepts the zero axis. Therefore, it is unlikely that this effect is significant.

Figure 6 shows the coefficient values from the generalized linear model. The intercept parameter combination is as follows: 0.25 Hz activation frequency, flexible backbone foil, 0.5 kPa maximum pressure, 0 cm s^{-1} flow speed, and 0% minimum pressure. Increasing minimum pressure alone decreased thrust, but increasing minimum pressure in the presence of flow speed increased thrust. Increasing maximum pressure alone increases thrust. Increasing maximum pressure and stiffness together (figure 6: blue box) again shows an interaction effect, where increasing the maximum pressure for the medium stiffness foil did not exhibit a large increase in thrust, whereas each increase in pressure for the stiff foil exhibited a larger increase in thrust. However, increasing maximum pressure in the presence of flow speed decreased thrust. Increasing frequency alone increases thrust for the flexible foil, with diminishing returns after 0.5 Hz. Increasing frequency and stiffness together (figure 6: green box) shows a linear interaction effect whereby by the medium and the stiff foil show a trend of increasing thrust with frequency, which stands in opposition to the individual effects of increasing stiffness without increasing frequency.

Finally, looking the interaction between frequency, stiffness, and maximum pressure (figure 6: gray box) shows the combination that increases thrust the second-most: 0.75 Hz, 1.0 kPa, and the stiffest backbone foil.

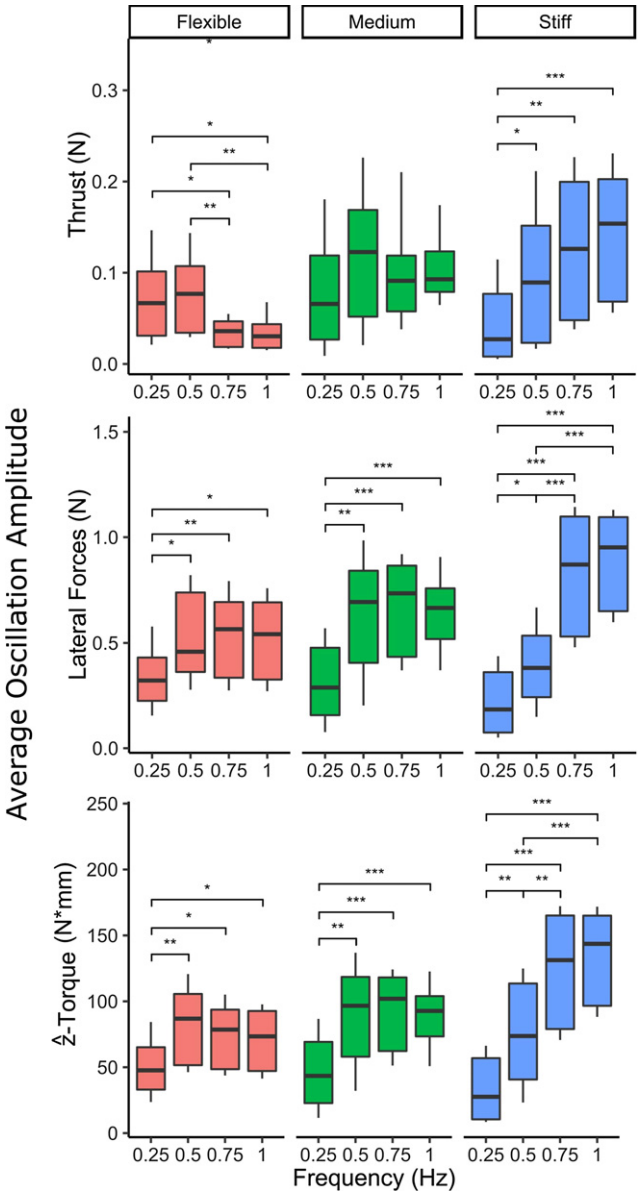

Figure 8. Average thrust, lateral force, and torque oscillation amplitudes. For the medium and stiff backbone foils, increasing frequency resulted in the same or higher values for thrust, lateral forces, and z-torque. $^{*}P < 0.05$, $^{**}P < 0.01$, $^{***}P < 0.001$.

The interaction between frequency and foil stiffness in particular is highlighted in figure 7. Increasing activation frequency for the flexible pneufish had no significant effect on thrust production. The medium stiffness pneufish generated the highest amount of thrust at 0.5 Hz, and then experienced reduced thrust at the two highest frequencies. The stiff pneufish experienced a significant increase in thrust between 0.25 Hz and the three other frequencies, but not between the other three frequencies themselves.

We analyzed peak-to-peak oscillation amplitude values for $F_{\hat{x}}$, $F_{\hat{y}}$, and $T_{\hat{z}}$. In the pneufish models, we observed a coupling between net thrust, lateral force, and z-torques (figure 8) such that no parameter combination resulted in an increase in thrust while simultaneously decreasing lateral forces or z-torques.

4. Discussion

The study by Jusufi *et al* (2017) described the development of a pneumatically-controlled fish-like model that was used to explore several general characteristics of aquatic propulsion. The development of this active-flapping model provided a new approach to understanding undulatory aquatic swimming. A number of previous studies using purely passive flapping models have provided many insights into the fundamental hydrodynamics of propulsion. However, passive models, incapable of actively bending, are not ideal biological models (Hemmati *et al* 2019, Quinn *et al* 2015, Dewey *et al* 2014, Shelton *et al* 2014, Lauder *et al* 2012). Although still a highly simplified experimental platform compared to more complex fish-like soft robotic systems (Katzschmann *et al* 2018, Zhu *et*

al 2019), active pneumatic control to bend a simplified plastic 'backbone' provides advantages for studying basic features of aquatic propulsion. For example, an active model system allows study of the extent to which co-contraction on each side of the body affects propulsion (Jusufi *et al* 2017). Furthermore, this active model considerably extends the capabilities of previous passive foil models of swimming (Lauder *et al* 2012, Shelton *et al* 2014) by allowing direct control of backbone curvature and amplitude and by introducing new and more complex control parameters such as pressure.

The Jusufi *et al* (2017) paper focused on analysis of thrust forces generated during swimming as a function of co-contraction phase, with experiments based on a physical model with one backbone stiffness, although different overall body stiffness was achieved by modulating soft actuator pressurization. Aquatic propulsion in fishes is also characterized by significant side-force generation (Tytell *et al* 2010) and fishes are believed to modulate stiffness as speed increases during swimming (McHenry *et al* 1995, Long 1998, Long *et al* 1994, Long *et al* 1996). Therefore one goal of this paper was to build upon the approach of Jusufi *et al* (2017) and study three separate model 'pneufish' each with a different stiffness central plastic backbone, and to additionally record and analyze side forces and torques generated by pneunet activation during locomotion. We formulated a statistical model with the goal of simplifying the presentation and interpretation of multiple effects involved in thrust-generation during locomotion (figure 6). Finally, we modified our control of pneunet inflation by substituting two pressure solenoid valves and a pressure sensor (used in Jusufi *et al* (2017)) with two digital pressure controllers. The digital pressure controllers allowed us to not only set the maximum pressure value for activation (which directly contributes to bending amplitude), but also the minimum pressure remaining in the pneunets when not activated, and the inflation rate. By changing the minimum pressure from zero, we are able to modulate the overall stiffness of the pneufish during activation and investigate the effects on amplitude and thrust production.

4.1. The relationship between pneufish amplitude, flow speed and net thrust

It is reasonable to speculate that frequency, maximum and minimum pressure, flow speed, and stiffness all impact thrust through amplitude. Either pushing a larger volume of water or pushing the same amount of water faster/more forcefully will produce more thrust. An imposed flow speed of 5.3 cm s^{-1} is not strong enough to decrease amplitude significantly. However, parameters that increase the frontal area, such as maximum pressure, will incur higher drag forces in the presence of the higher flow, and vice versa (figure 6). Increasing stiffness decreases amplitude, and consequently thrust, while maximum pressure will increase both. Increasing frequency in the flexible foil probably increases thrust by pushing the small or small volume of water faster, but it experienced diminishing returns. The peak at 0.5 Hz could possibly be due to resonance in the plastic backbone foil.

Non-zero flow introduces realistic, induced drag into the system. As we measured net thrust, a system with higher drag will generally decrease thrust. However, thrust increases with minimum pressure in a non-zero flow situation, which stands in opposition to the individual effects of both minimum pressure and non-zero flow. Again, this can be explained partially through amplitude. Increasing minimum pressure provides an antagonistic force that resists bending. As Jusufi *et al* (2017) demonstrated, co-activation increases overall stiffness, which decreases amplitude. In the situation of non-zero flow, employing active stiffness modulation to decrease amplitude serves to lessen the incurred drag, thereby increasing net thrust.

Given how important oscillation amplitude is, why, then, was it not included in the best-fit model? The linear regression model that predicted net thrust solely based on amplitude indicated amplitude was a significant predictor ($p = 1.1 \times 10^{-13}$, $R^2 = 0.17$). However, the AIC analysis removed only amplitude in favor of the model presented (supp. table 1). Our conclusion is, amplitude is a key driver of thrust production, but is not solely capable of explaining the variance present in thrust. AIC analysis likely removed amplitude because it was at least somewhat correlated with other predictors and not fully capable of explaining the variance.

Lastly, it is important to note that in the presence of non-zero flow, amplitude plays a much larger role, as it is correlated with increased frontal area. When the simple amplitude model was expanded to include flow speed as a predictor and the interaction, R^2 increased to 0.55. These two indicators and their interaction alone are capable of explaining half of the variance present in the data, because amplitude has complicated effects that vary in the presence of the flow speed.

4.2. The importance of stiffness–frequency interactions

Using a linear statistical model allows us to visualize the contribution of each control parameter on pneufish swimming performance. More importantly, the linear regression model suggests which parameter interactions are most influential and which have a minimal contribution to thrust production (as noted by a confidence interval intercepting the 0 mN line in figure 6). The benefit of using such a model and presenting a coefficients plot is the easy visualization of parameter effects and the reduced need for a multitude of graphs for each individual parameter. The parameter combination that maximized thrust was

simply the most flexible foil, lowest frequency, and the highest maximum pressure—maximizing amplitude and pushing water for the longest duration possible (figure 6). The second best way to maximize thrust was to activate the stiffest foil with the highest pressure and second-highest frequency in the parameter space.

The statistical model reveals a strong interaction between stiffness, conferred both by the backbone foil stiffness and pneunet air pressure, and activation frequency. Specifically, increasing the frequency for the most flexible pneufish did not result in any significant changes or increases in thrust production. However, with the stiffest pneufish, we observe a significant increase in thrust production between the slowest frequency and the higher frequencies.

This parallels several observations and assumptions in fish studies. McHenry *et al* (1995) suggested that fish need to increase their overall flexural stiffness, most likely through increased bilateral muscle activation, in order to fully capitalize on higher frequencies in swimming. This is thought to be related to natural resonance frequencies. Similarly, Shelton *et al* (2014), hypothesized from passively swimming foil data that fish should be able to modulate their swimming motions (heave/pitch) and overall body stiffness in order to adjust their swimming performance to suit their current situational needs.

The statistical model presented here suggests the same stiffness–frequency interaction predicted from previous studies of dead fish and other robotic models, suggesting that this interaction is an underlying necessity of swimming at variable speeds and frequencies (McHenry *et al* 1995, Barrett *et al* 1999, Mcletchie, 2003, Long *et al* 1996, Lauder 2011, Colgate and Lynch 2004, MacIver *et al* 2004). To swim more quickly (or to produce more thrust), one must modulate the total flexural stiffness of the body. The exact nature of this relationship (linear or non-linear) is as yet undetermined, as this cannot be estimated accurately from the three stiffness points included in this study. Nonetheless, this result can be applied to future robotic models.

4.3. Lateral forces in aquatic locomotion

Ideally, fish would minimize the magnitude of lateral force oscillation amplitude during swimming, thus minimizing the amount of energy spent in directions other than that of the desired travel. In a study looking at the forces produced by a live mackerel using particle image velocimetry (PIV) to visualize flow in the wake, Nauen and Lauder (2002) found that lateral forces were twice as high as the forward thrust, and suggested that such a ratio of lateral force to thrust force is an necessary feature of undulatory locomotion. Likewise, Xiong and Lauder (2014) analyzed center of mass (COM) oscillation for fish with three distinct, preferred swimming modes: bluegill (carangiform), eel (anguilliform), and knifefish (anal fin undulatory). They found that sway, or the amount of lateral oscillation, of the COM was highest in eels, but that lateral COM oscillation was present in all species at higher speeds, suggesting that lateral COM motion is an inherent feature of generating undulatory movement and may limit the total efficiency of locomotion. Furthermore, Mignano *et al* (2019) and Wen *et al* (2018) studied the role of median fish fins in propulsion and proposed that these fins, if their motion is appropriately phased, can act to reduce overall lateral force oscillation magnitude on the body. These results provide general support for the idea that lateral forces are a necessary feature of body undulatory locomotion in fishes, and that although they may contribute to stability and maneuverability of an undulatory swimmer, they also may increase swimming costs (Dickinson *et al* 2000, Lauder *et al* 2002).

We analyzed the pneufish parameter space for a combination that maximized peak-to-peak amplitude in thrust while minimizing side forces, and we did not find one. In the pneufish model, forward thrust and lateral forces increase linearly, but the lateral forces are roughly five times the magnitude of the thrust force (figure 8). In addition, this relationship was roughly consistent across pneufish of various stiffnesses.

Without a means of measuring power efficiency in our pneumatic apparatus, we can use this ratio as a rough means of comparing of swimming performance of the pneufish to fishes. The pneufish displays a considerably greater ratio of lateral to thrust force generation (nearly 5:1) whereas fishes swimming with an undulatory body wave typically show a 2:1 ratio (see Nauen and Lauder (2002)). This indicates that our model is most likely a substantially less-efficient swimmer than swimming fish like mackerel or bluegill. However, it is important to note that this is not a fully undulatory model (as seen in figure 3, the pneufish 'flaps' rather than undulates), and we suspect that with a wavelength greater than 1, the lateral forces generated by a full sinusoidal curve could cancel in part, potentially reducing the lateral:forward thrust ratio from 5:1 to a more fish-like 2:1. Future experiments explore the possibility of generating a wavelength greater than 1 by using multiple sequential pneunet pairs.

4.4. Pneufish as a swimming model

The pneufish is an actively-swimming soft-robotic platform, and it fills a niche space between passive, foil-only systems that are quickly produced and controlled but not actively swimming, and more fish-like robotic systems that are complicated to produce and control, but actively swimming. This study has shown that the pneufish model is capable of producing active swimming behavior simulating parameter interactions suggested to underlie fish propulsion.

Our results can also be compared to the bio-inspired model of Park *et al* (2014) in which stiffness is altered using the backbone component, rather than via pneumatic muscles. Similar to our results, they found that higher amplitudes resulted in higher thrust, and that being more flexible at lower frequencies resulted in higher thrust production compared to higher stiffness. Conversely, they found that higher frequencies, with amplitude held constant, resulted in higher thrust. This was not the case for our model since amplitude, a non-controlled variable, decreased as we increased frequency. Despite that difference, our pneufish model shows similar results to that of hard-robotic models, which suggests that both approaches are focusing on key parameters that underlie undulatory fish-like propulsion.

However, the pneufish model used here possesses several limitations. Pneunets are made individually and placement of the pneunets is done by hand. While great care is taken to ensure each pneunet is identical and symmetrically placed on the backbone foil, some small variation does exist and is likely a small source of noise and variance in the data. Furthermore, the digital pressure regulators pose most of the performance limitations. They are ineffective at delivering sufficient and timely air pressure to the pneunets at frequencies higher than 1 Hz. At the moment, they afford fine-tuned control of pneumatic actuation, but the ability to actuate pressure fluctuations and deliver them to the pneunet at higher frequencies of 2–5 Hz would allow study of higher performance fish-like locomotion. Lastly, unlike previous foil-based studies, power and efficiency cannot be calculated directly due to the absence of a motor, the pneunets moving air, and the compliance of the various flexible components in the system.

Despite these limitations, we believe the pneufish model presented here could be usefully extended by incorporating multiple individually controlled pneunets with a longer 'body'. This will allow better control of lateral forces, a more fish-like undulatory wave with a shorter wavelength, and a consequent increase in swimming performance. This model would permit us to address more specific hypotheses about the function of individual segmented contractile elements, assess the relationship between wavelength and both lateral and thrust force generation, and permit evaluation of more complex control programs such as those used during maneuvering and burst swimming behaviors.

Acknowledgments

This work was supported by the Department of Organismic and Evolutionary Biology at Harvard University, the Ashford Foundation, and the Office of Naval Research (Tom McKenna, Program Manager, ONR 341), Grant No. N00014-15-1-2234, as well as the Swiss National Science Foundation, Grant No. P2SKP3_158677, and the Cyber Valley Research Fund (Grant No. CyVy-RF-2019-08) and the Max Planck Society. Special thanks to Arben Kalziqi for his assistance and guidance with Mathematica, and Dave G Matthews and Robin Thandiackal for many helpful discussions.

ORCID iDs

Z Wolf https://orcid.org/0000-0001-7607-459X
A Jusufi https://orcid.org/0000-0003-4250-2984
D M Vogt https://orcid.org/0000-0003-1286-7034
G V Lauder https://orcid.org/0000-0003-0731-286X

References

Bainbridge R 1958 The speed of swimming of fish as related to size and to the frequency and amplitude of the tail beat *J. Exp. Biol.* **35** 109–33

Barrett D, Triantafyllou M S, Yue D, Grosenbaugh M and Wolfgang M 1999 Drag reduction in fish-like locomotion *J. Fluid Mech.* **392** 183–212

Colgate J E and Lynch K M 2004 Mechanics and control of swimming: a review *IEEE J. Ocean. Eng.* **29** 660–73

Coral W, Rossi C, Curet O M and Castro D 2018 Design and assessment of a flexible fish robot actuated by shape memory alloys *Bioinspiration Biomimetics* **13**

Dewey P A, Quinn D B, Boschitsch B M and Smits A J 2014 Propulsive performance of unsteady tandem hydrofoils in a side-by-side configuration *Phys. Fluids* **26** 041903

Dickinson M, Farley C T, Full R J, Koehl M A, Kram R and Lehman S 2000 How animals move: an integrative view *Science* **288** 100–6

Drucker E G 1996 The use of gait transition speed in comparative studies of fish locomotion *Am. Zool.* **36** 555–66

Feilich K L and Lauder G V 2015 Passive mechanical models of fish caudal fins: effects of shape and stiffness on self-propulsion *Bioinspiration Biomimetics* **10** 036002

Fish F and Lauder G V 2006 Passive and active flow control by swimming fishes and mammals *Annu. Rev. Fluid Mech.* **38** 193–224

Gelman A and Hill J 2006 *Data Analysis Using Regression and Multilevel/Hierarchical Models* (New York: Cambridge University Press)

Gravish N and Lauder G V 2018 Robotics-inspired biology *J. Exp. Biol.* **221** 1–8

Hemmati A, Van Buren T and Smits A J 2019 Effects of trailing edge shape on vortex formation by pitching panels of small aspect ratio *Phys. Rev. Fluids* **4** 033101

Jusufi A, Vogt D M, Wood R J and Lauder G V 2017 Undulatory swimming performance and body stiffness modulation in a soft robotic fish-inspired physical model *Soft Robot.* **4** 202–10

Katzschmann R K, DelPreto J, MacCurdy R and Rus D 2018 Exploration of underwater life with an acoustically controlled soft robotic fish *Sci. Robot.* **3** eaar3449

Lauder G V 2011 Swimming hydrodynamics: ten questions and the technical approaches needed to resolve them *Exp. Fluids* **51** 23–35

Lauder G V 2015 Fish locomotion: recent advances and new directions *Ann. Rev. Mar. Sci.* **7** 521–45

Lauder G V, Flammang B and Alben S 2012 Passive robotic models of propulsion by the bodies and caudal fins of fish *Integr. Comp. Biol.* **52** 576–87

Lauder G V, Lim J L, Shelton R M, Witt C, Anderson E J and Tangorra J L 2011 Robotic models for studying undulatory locomotion in fishes *Mar. Technol. Soc. J.* **45** 41–55

Lauder G V, Nauen J C and Drucker E G 2002 Experimental hydrodynamics and evolution: function of median fins in ray-finned fishes *Integr. Comp. Biol.* **42** 1109–17

Li K, Jiang H, Wang S and Yu J 2018 A soft robotic fish with variable-stiffness decoupled mechanisms *J. Bionic Eng.* **15** 599–609

Liao J C 2004 Neuromuscular control of trout swimming in a vortex street: implications for energy economy during the Karman gait *J. Exp. Biol.* **207** 3495–506

Long J H, Nipper K S, Long J H Jr and Nipper K S 1996 The importance of body stiffness in undulatory propulsion1 *Am. Zool.* **36** 678–94

Long J H Jr 1998 Muscles, elastic energy, and the dynamics of body stiffness in swimming eels *Am. Zool.* **38** 771–92

Long J H Jr 2012 *Darwin's Devices: What Evolving Robots Can Teach Us about the History of Life and the Future of Technology* vol 52 (New York: Basic Books) https://doi.org/10.1093/icb/ics107

Long J H Jr, McHenry M and Boetticher N 1994 Undulatory swimming: how traveling waves are produced and modulated in sunfish (*Lepomis gibbosus*) *J. Exp. Biol.* **192** 129–45

Lucas K N, Thornycroft P J M, Gemmell B J, Colin S P, Costello J H and Lauder G V 2015 Effects of non-uniform stiffness on the swimming performance of a passively-flexing, fish-like foil model *Bioinspiration Biomimetics* **10** 056019

MacIver M A, Fontaine E and Burdick J W 2004 Designing future underwater vehicles: principles and mechanisms of the weakly electric fish *IEEE J. Ocean. Eng.* **29** 651–9

McHenry M, Pell C and Long J H Jr 1995 Mechanical control of swimming speed: stiffness and axial wave form in undulating fish models *J. Exp. Biol.* **198** 2293–305

Mcletchie K-M W 2003 Drag reduction of an elastic fish model *Oceans 2003. Celebrating the Past… Teaming Toward the Future* **5** pp SP2938–SP2944

Mignano A P, Kadapa S, Tangorra J L and Lauder G V 2019 Passing the wake: using multiple fins to shape forces for swimming *Biomimetics* **4** 1–23

Mosadegh B, Polygerinos P, Keplinger C, Wennstedt S, Shepherd R F, Gupta U, Shim J, Bertoldi K, Walsh C J and Whitesides G M 2014 Pneumatic networks for soft robotics that actuate rapidly *Adv. Funct. Mater.* **24** 2163–70

Nauen J C and Lauder G V 2002 Hydrodynamics of caudal fin locomotion by chub mackerel, *Scomber japonicus* (Scombridae) *J. Exp. Biol.* **205** 1709–24

Park Y J, Huh T M, Park D and Cho K J 2014 Design of a variable-stiffness flapping mechanism for maximizing the thrust of a bio-inspired underwater robot *Bioinspiration Biomimetics* **9** 036002

Quinn D B, Lauder G V and Smits A J 2015 Maximizing the efficiency of a flexible propulsor using experimental optimization *J. Fluid Mech.* **767** 430–48

R Core Team 2013 R: a language and environment for statistical computing http://r-project.org/

Schneider C A, Rasband W S and Eliceiri K W 2012 NIH Image to ImageJ: 25 years of image analysis *Nat. Methods* **9** 671–5

Shadwick R E and Gemballa S 2005 Structure, kinematics, and muscle dynamics in undulatory swimming *Fish Physiology* vol 23 (San Diego: Academic) pp 241–80

Shelton R M, Thornycroft P J M and Lauder G V 2014 Undulatory locomotion of flexible foils as biomimetic models for understanding fish propulsion *J. Exp. Biol.* **217** 2110–20

Souri H *et al* 2020 Wearable and stretchable strain sensors: materials, sensing mechanisms, and applications, *Adv. Int. Syst.* in preparation

Tytell E D 2006 Median fin function in bluegill sunfish *Lepomis macrochirus:* streamwise vortex structure during steady swimming *J. Exp. Biol.* **209** 1516–34

Tytell E D and Lauder G V 2004 The hydrodynamics of eel swimming II. Effect of swimming speed *J. Exp. Biol.* **207** 3265–79

Tytell E D, Hsu C-Y, Williams T L, Cohen A H and Fauci L J 2010 Interactions between internal forces, body stiffness, and fluid environment in a neuromechanical model of lamprey swimming *Proc. Natl Acad. Sci.* **107** 19832–7

Venables W and Ripley B 2013 *Modern Appplied Statistics with S-PLUS* 4th edn (Berlin: Springer)

Wen L and Lauder G V 2013 Understanding undulatory locomotion in fishes using an inertia-compensated flapping foil robotic device *Bioinspiration Biomimetics* **8** 046013

Wen L, Ren Z, Di Santo V, Hu K, Yuan T, Wang T and Lauder G V 2018 Understanding fish linear acceleration using an undulatory biorobotic model with soft fluidic elastomer actuated morphing median fins *Soft Robot.* **5** 375–88

Wolfram Research Inc. 2019 Mathematica 11.0 http://wolfram.com

Wright B, Vogt D M, Wood R J and Jusufi A 2019 Soft sensors for curvature estimation under water in a soft robotic fish *2019 2nd IEEE Int. Conf. on Soft Robotics (RoboSoft)* pp 367–71

Xiong G and Lauder G V 2014 Center of mass motion in swimming fish: effects of speed and locomotor mode during undulatory propulsion *Zoology* **117** 269–81

Zhou W and Li Y 2020 Modeling and analysis of soft pneumatic actuator with symmetrical chambers used for bionic robotic fish *Soft Robot.* **7** 168–78

Zhu J, White C, Wainwright D K, Di Santo V, Lauder G V and Bart-Smith H 2019 Tuna robotics: a high-frequency experimental platform exploring the performance space of swimming fishes *Sci. Robot.* **4** 1–12

Ziegler M, Hoffmann M, Carbajal J P and Pfeifer R 2011 Varying body stiffness for aquatic locomotion *Proc. IEEE Int. Conf. on Robotics and Automation* pp 2705–12